Sub-pixel Target Mapping from Soft-classified, Remotely Sensed Imagery

Peter M. Atkinson

Abstract

A simple, efficient algorithm is presented for sub-pixel target mapping from remotely-sensed images. Following an initial random allocation of "soft" pixel proportions to "hard" sub-pixel binary classes, the algorithm works in a series of iterations, each of which contains three stages. For each pixel, for all sub-pixel locations, a distance-weighted function of neighboring sub-pixels is computed. Then, for each pixel, the sub-pixel representing the target class with the minimum value of the function, and the sub-pixel representing the background with the maximum value of the function are found. Third, these two sub-pixels are swapped if the swap results in an increase in spatial correlation between sub-pixels. The new algorithm predicted accurately when applied to simple simulated and real images. It represents an accessible tool that can be coded and applied readily by remote sensing investigators.

Introduction

Land cover is a fundamental variable that underpins much scientific research. For example, data on land cover are required to provide boundary conditions for climate models (e.g., global circulation models (van den Hurk *et al.*, 2003)) and hydrological and hydraulic models (e.g., the provision of spatially distributed friction coefficients) (Mason *et al.*, 2003; Wilson and Atkinson, 2003). Despite their importance, informative, and accurate data on land cover are both difficult and expensive to provide. Therefore, much of the land cover data currently being used in scientific research are of inadequate quality. For example, much land cover data may be (a) incomplete spatially, (b) out-of-date, or (c) inaccurate. Remote sensing is capable of providing synoptic and complete coverage of potentially very large areas. Furthermore, multi-temporal images can be used to monitor changes in land cover over time. For these reasons, remote sensing has been of great value for land cover mapping and monitoring.

Despite the obvious utility of remote sensing for land cover mapping, many problems remain. For example, it is often difficult to ensure appropriate spatial coverage at an appropriate spatial resolution. Furthermore, it can be difficult to provide temporal coverage with sufficient frequency for monitoring purposes because of the limited revisit time of the satellite, or *obscuration* of the scene due to persistent cloud cover (e.g., in tropical regions). Even where sufficient spatial and temporal coverage is possible, the accuracy of classification algorithms is frequently limited to around 80 to 90 percent (Congalton, 1991; Foody, 2002). Increasing the accuracy of land cover classification has been the subject of intensive research for many years (Justice and Townshend, 1981; Foody, 2002). One limitation to the accuracy of land cover classification that is implicit, and always present, in remotely sensed images is the spatial resolution. While complete cover may be provided for an area of interest, the *sample* can never be complete; increasing the spatial resolution of the sensor will generally reveal greater detail.

Spatial resolution has been the subject of research in remote sensing for many years because it forms a fundamental scale of measurement (Woodcock and Strahler, 1987; Atkinson and Tate, 2000; Tate and Atkinson, 2001). The spatial variation observed in remotely sensed imagery is a function of both the property of interest (i.e., the real world) and the sampling framework (i.e., the ensemble of sensor characteristics including the spatial resolution). Researchers have sought to evaluate the effect of spatial resolution on detectable spatial variation as characterized by functions such as the local variance (Woodcock and Strahler, 1987) and variogram (Jupp *et al.*, 1987, 1988; Curran and Atkinson, 1998). Furthermore, researchers have attempted to find a suitable means of selecting a spatial resolution given knowledge of functions such as the variogram (Atkinson and Curran, 1997). Such research demonstrated that spatial resolution has a fundamental effect on the spatial variation in remotely sensed imagery.

Early techniques for land cover classification from remotely sensed imagery focused on hard classification (both supervised and unsupervised) in which each pixel is allocated to one class (Thomas *et al.*, 1987). About two decades ago, researchers began to realize that for most remotely-sensed scenes, hard classification is inappropriate (Bezdek *et al.*, 1984; Adams *et al.*, 1985; Gillespie, 1992). Many pixels in remotely sensed images represent more than one land cover class on the ground. Such *mixed pixels* occur where the frequency of spatial variation in land cover is greater than or equal to the frequency of sampling afforded by the sensor's spatial resolution (Woodcock and Strahler's (1987), L-resolution case). However, a proportion of pixels will be mixed even where the spatial resolution is fine relative to the land cover variation (H-resolution case) because some pixels inevitably straddle boundaries between scene *objects*.

The existence of mixed pixels led to the development of several approaches for soft (often termed *fuzzy* in the remote sensing literature) classification in which each pixel is allocated to all classes in varying proportions. Examples of techniques for soft classification applied to remotely-sensed

Department of Geography, University of Southampton, Highfield, Southampton SO17 1BJ, UK (pma@soton.ac.uk).

Photogrammetric Engineering & Remote Sensing
Vol. 71, No. 7, July 2005, pp. 839–846.

0099-1112/05/7107–0839/$3.00/0

imagery include the linear mixture model (Adams *et al.*, 1985; Foody and Cox, 1994; Garcia-Haro *et al.*, 1996), fuzzy *c*-means classification (Bezdek, 1981; Bezdek *et al.*, 1984), and feed-forward, back-propagation (FFBP) neural networks trained on class proportions (Benediktsson *et al.*, 1990; Paola and Schowengerdt, 1995; Atkinson and Tatnall, 1997; Atkinson *et al.*, 1997), among many others. More recently, softened support vector machines have also become popular (Brown *et al.*, 1999).

All of the above techniques may be used to provide a soft classification of land cover that is both more informative and potentially more accurate than the equivalent hard classification. However, while the proportions of each land cover within each pixel may be predicted, the spatial location of each land cover within each pixel is not. For example, a soft classifier may predict 60 percent woodland within a pixel. This is undoubtedly more informative than *woodland* as predicted by a hard classifier. However, it would also be useful to know *where*, within the pixel, the woodland is located spatially. That goal, referred to here as *sub-pixel mapping*, is the subject of this paper. It amounts to transforming multispectral (i.e., multivariate) data into spatial (univariate) data. While no new information is created, it does result in an increase in spatial resolution above that achieved with hard (and soft) classification of the original remotely sensed imagery.

There exist many different potential techniques for sub-pixel mapping from remotely sensed imagery. Perhaps the simplest approach involves converting a hard-classified image into the vector data model by replacing class object boundaries with vectors. Generalizing these vectors will produce sub-pixel spatial information on land cover, albeit of limited value (Atkinson, 1997). Foody (1998) evaluated an interpolation-based technique for predicting the boundary of a lake with sub-pixel geometric precision. However, as for the line generalization approach above, this approach was under-constrained. Specifically, the resulting contour line (representing the boundary between lake and not lake) need not honor any prior model or expectation (e.g., soft land cover proportions, if these are known).

More recently, Aplin and Atkinson (2001) developed a technique for converting the output from a per-pixel soft-classification of land cover into a per-parcel hard classification of land cover objects. Landline vector data from the Ordnance Survey were used to constrain the placement of the soft proportions within each pixel. However, the technique depends on the availability of a vector or polygon database making the technique redundant for (a) less developed areas of the world, and (b) updating the vector database.

Several authors have attempted sub-pixel mapping directly from multispectral remotely-sensed imagery. For example, in a series of papers, Schneider (1993, 1999) and Steinwendner *et al.* (1998) document a technique for sub-pixel mapping of linear features based on a 3 pixel by 3 pixel kernel, or moving window. This approach was extended to include neural network prediction of vector boundaries, but is restricted to remotely sensed images and the detection of linear features. Flack *et al.* (1994) developed a technique based on the Hough transform for, first, detecting linear features in remotely sensed images of agricultural scenes and, second, un-mixing the signal on either side of the boundary. Again, the technique is suitable for application to linear features in unprocessed, remotely sensed images.

The author (Atkinson, 1997) suggested sub-pixel mapping based solely on the output from a soft classification. The idea proposed was to convert soft land cover proportions to hard (per-sub-pixel) land cover classes (that is, at a finer spatial resolution) by maximizing the spatial dependence or spatial correlation between neighboring sub-pixels under the constraint that the original pixel proportions were maintained (Atkinson, 1997). Spatial dependence is the likelihood that observations close together are more alike than those that are further apart (Matheron, 1965; Goovaerts, 1997; Chiles and Delfiner, 1999). This objective is reasonable where the land cover target of interest is larger than the pixels in the imagery. The algorithm produced excellent results for simple shapes such as a circle and a torus. The algorithm was also applied to a complex arrangement of multiple-class land cover objects found in a Systéme Pour L'Observation de la Terre (SPOT) High Resolution Visible (HRV) image of the New Forest, Hampshire.

The algorithm proposed by Atkinson (1997) predicted sub-pixel class on the basis of neighboring pixels. Two algorithms have subsequently been proposed that also utilize the information in neighboring pixels. Verhoeye and De Wulf (2002), building on the earlier work of Atkinson (1997), attempted to allocate sub-pixel hard classes using a technique similar to the spectral mixture model. The pixel proportion constraints were built into the mixture model, and a solution was achieved by least squares approximation. Zhan *et al.* (2002) implemented an inverse-distance weighting algorithm to interpolate the unknown sub-pixel class from neighboring pixel-level land cover proportions. To locate the "point" meant to represent the location of the neighboring pixel; both the corners and centers of neighboring pixels were used.

Recently, Tatem *et al.* (2001a) developed an alternative to the above algorithms in which sub-pixels are compared to neighboring sub-pixels. The advantage of comparing sub-pixels to sub-pixels is that the draw of a neighboring pixel is not static from iteration to iteration. Specifically, Tatem *et al.* (2001a) developed a Hopfield neural network (HNN) technique (Hopfield and Tank, 1985) for sub-pixel target mapping. The HNN is an optimization tool in which all neuron outputs are connected to all neuron inputs. To solve the sub-pixel mapping problem, with the pixel proportions as initial conditions, the HNN architecture must be such that all sub-pixels in the target image are represented by one neuron or node in the HNN. The sub-pixel class allocations are initialized randomly. The HNN is then set up to minimize an energy function which comprises a goal and constraints:

$$E = k_1 G + k_2 C + b \quad (1)$$

where the goal G is to increase the spatial correlation between neighboring sub-pixels, the constraint C is that the original class proportions per-pixel are maintained in the sub-pixel land cover map, k_1 and k_2 are weighting coefficients, and b is a bias term. The HNN was applied initially to detect targets (two-class problem) (Tatem *et al.*, 2001a), but eventually extended to sub-pixel land cover mapping (multiple-class problem) (Tatem *et al.*, 2001b).

The HNN has been demonstrated to be a useful and accurate tool for sub-pixel mapping. However, alternative classes of algorithm remain to be investigated. One, in particular, stands out as an obvious candidate, i.e., the adoption of a geographical pixel-swapping algorithm to allow the comparison of sub-pixels with sub-pixels. In the present paper, a simple pixel-swapping algorithm is described which is capable of producing sub-pixel maps from binary input images. This simple algorithm initially allocates hard binary classes randomly to sub-pixels. Thereafter, the spatial *location* of the hard classes is altered (pixel-swapping), rather than the attribute value at each location (as with the HNN). The algorithm is similar in concept to the set of techniques known as simulated annealing in a geostatistical framework (Deutsch and Journel, 1998). The new pixel-swapping algorithm for sub-pixel mapping is described in the next section.

Methods

The simple algorithm presented and described here is both simple and efficient.

Pixel-swapping Algorithm

The pixel-swapping algorithm is designed to receive, as input, an image of land cover proportions in $K = 2$ classes (probably obtained by application of a soft classifier to a remotely sensed image). First, the pixel-level land cover proportions are transformed into sub-pixel hard land cover classes. Thus, if 10 sub-pixels by 10 sub-pixels are to be mapped within each pixel, a land cover proportion of 57 percent would mean that 57 sub-pixels were allocated to that class. Second, these sub-pixels are allocated randomly within each pixel. Once allocated, only the spatial arrangement of the sub-pixels can vary, not the actual attribute values. Furthermore, the number of sub-pixels allocated within each pixel remains fixed. However, this is not a constraint in the sense of the HNN algorithm; the proportions at the pixel level cannot vary.

Given the above random initialization, the objective is to vary the spatial arrangement of the sub-pixels in such a way that the spatial correlation between neighboring sub-pixels (both *within* and, perhaps more importantly, *between* pixels) is maximized given that the pixel-level proportions cannot vary. There are many possible approaches. The one adopted here is described below, and it is comprised of three basic steps.

First, for every sub-pixel the attractiveness A_i of a pixel i is predicted as a distance-weighted function of its $j = 1,2, \ldots, J$ neighbors:

$$A_i = \sum_{j=1}^{j} \lambda_{ij} z(\mathbf{x}_j) \tag{2}$$

where $z(\mathbf{x}_j)$ is the (binary) class of the j^{th} pixel at location $\mathbf{x}_j$, and λ_{ij} is a distance-dependent weight predicted as:

$$\lambda_{ij} = \exp\left(\frac{-h_{ij}}{a}\right) \tag{3}$$

where h_{ij} is the distance between the location $\mathbf{x}_i$ of pixel i for which the attractiveness is desired, the location $\mathbf{x}_j$ of a neighboring pixel j, and a is the non-linear parameter of the exponential model. The exponential weighting function chosen here is essentially arbitrary, and several alternatives such as a simple inverse distance weighting function or the Gaussian model could be used instead. The choice of a non-linear parameter and the number of nearest neighbors are both important considerations, and will be revisited in the discussion.

Second, once the attractiveness of each sub-pixel location has been predicted based on the current arrangement of sub-pixel classes, the algorithm ranks the scores on a pixel-by-pixel basis. For each pixel, the least attractive location at which the sub-pixel is currently allocated to a "1" (i.e., a "1" surrounded mainly by "0"s) is stored:

$$\text{candidate A} = (\mathbf{x}_i : A_i = \min(A) \big| z(\mathbf{x}_i) = 1). \tag{4}$$

Similarly, the most attractive location at which the pixel is currently allocated to a "0" (i.e., a "0" surrounded mainly by "1"s) is also stored:

$$\text{candidate B} = (\mathbf{x}_j : A_j = \max(A) \big| z(\mathbf{x}_j) = 0). \tag{5}$$

Third, sub-pixel classes are swapped on the following basis. If the attractiveness of the least attractive location is less than that of the most attractive location, then the classes are swapped for the sub-pixels in question:

$$\left.\begin{matrix} z(\mathbf{x}_i) = 0 \\ z(\mathbf{x}_j) = 1 \end{matrix}\right\} \quad \text{if} \quad A_i < A_j \,. \tag{6}$$

If it is more attractive, no change is made.

The above three-stage process is repeated such that a solution is approached iteratively. The process can be stopped either at a fixed number of iterations or when the algorithm converges on a solution. The algorithm is simple and fast. The basic steps involved in the algorithm are given below:

1. Allocate sub-pixels to classes based on the pixel-level proportions.
2. For each iteration:
    a. For each pixel:
        i. For each sub-pixel within the pixel:
            1. For each neighboring sub-pixel within a window
                a. calculate A per sub-pixel.
            2. Find minimum attractiveness A_i for all sub-pixels currently allocated to 1 (i.e., ($A_i = \min(A) | z(\mathbf{x}_i) = 1$)).
            3. Find maximum attractiveness A_j for all sub-pixels currently allocated to 0 (i.e., ($A_j = \max(A) | z(\mathbf{x}_j) = 0$)).
        ii. If $A_i < A_j$
            1. Swap the single pair of sub-pixel allocations.

Data

Four data sets were used to evaluate the proposed algorithm, and are described in this section.

Simple Targets

To test the performance of the algorithm two 35 sub-pixel by 35 sub-pixel target images of simple geometric shapes (circle and linear feature) were simulated using the Splus™ software. These shapes are shown in Figure 1a and Figure 2a. These images were aggregated into pixels of size 7 sub-pixels by 7 sub-pixels to form pixel-level images of 5 pixels by 5 pixels (Figure 1b and Figure 2b). These images of proportions were used to simulate (i.e., used in place of) real soft-classified remotely sensed images of land cover proportions. These images represent the sole input to the algorithm.

Polygonal Target

The most obvious application for the algorithm presented (i.e., spatial clustering of a *binary* field) is target detection in remotely sensed images. To test the algorithm beyond the simple shapes described above, a more *realistic* irregular polygon shape was created using the locator command in Splus™ (Figure 3a). This shape might correspond to a real feature (e.g., a large complex building or an asphalt parking lot) in a remotely sensed image (e.g., Landsat Thematic Mapper image with a spatial resolution of 30 m by 30 m). Furthermore, it represents a more complex geometry than the circle and linear features. In particular, it has two concave sides that make the feature more difficult to recreate using the algorithm. The image of the irregular polygon (Figure 3a) was degraded to a coarser spatial resolution to create an image of proportions (hypothetically of some target) with pixels of 7 sub-pixels by 7 sub-pixels (Figure 3b).

Ikonos Imagery

An Ikonos multispectral image with a spatial resolution of 4 m acquired on 30 August 2000 of Chandler's Ford and Eastleigh in Hampshire, UK was used to evaluate the algorithm. A small sub-image of 256 pixels by 256 pixels was extracted from the original image, representing an agricultural area just north of Chandler's Ford. The sub-image was classified using a maximum likelihood classifier trained using large regions of interest (polygons) of training data on three classes: cereals, grassland, and woodland. For the present purpose, the cereals

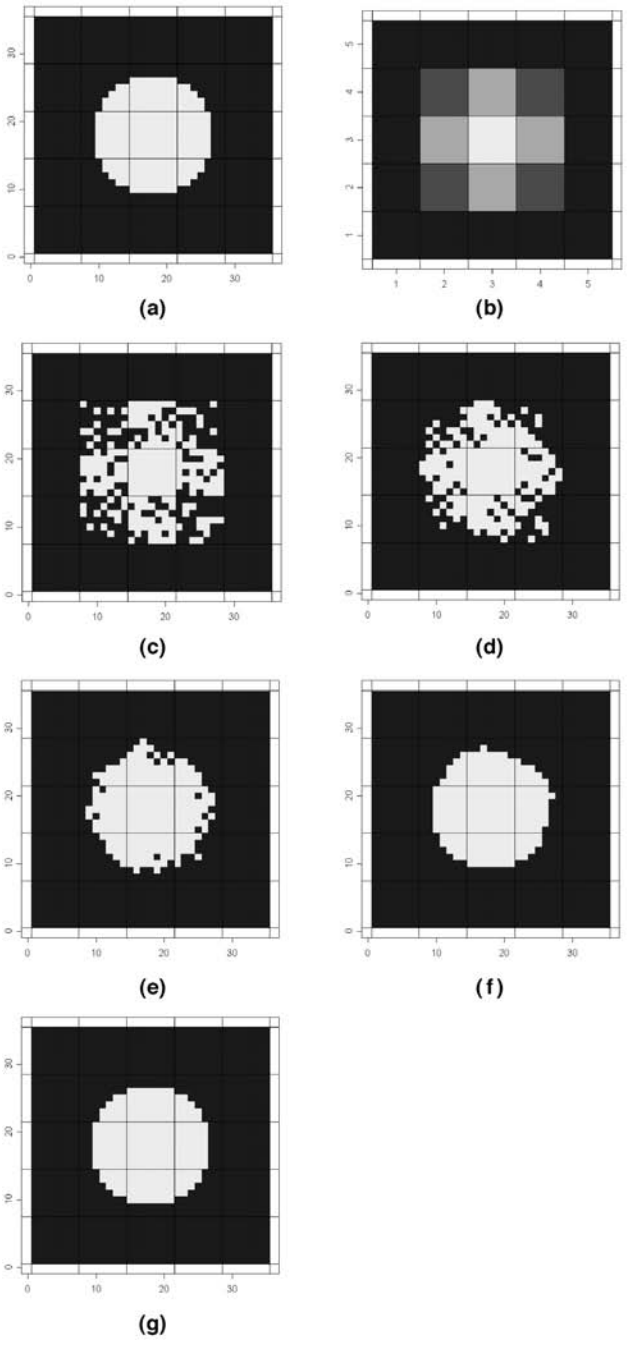

Figure 1. Sub-pixel mapping of a circle: (a) test image, (b) image of proportions input to the algorithm, (c) random initial allocation to sub-pixels, (d) solution after four iterations, (e) solution after 8 iterations, (f) solution after 12 iterations, and (g) solution after 16 iterations.

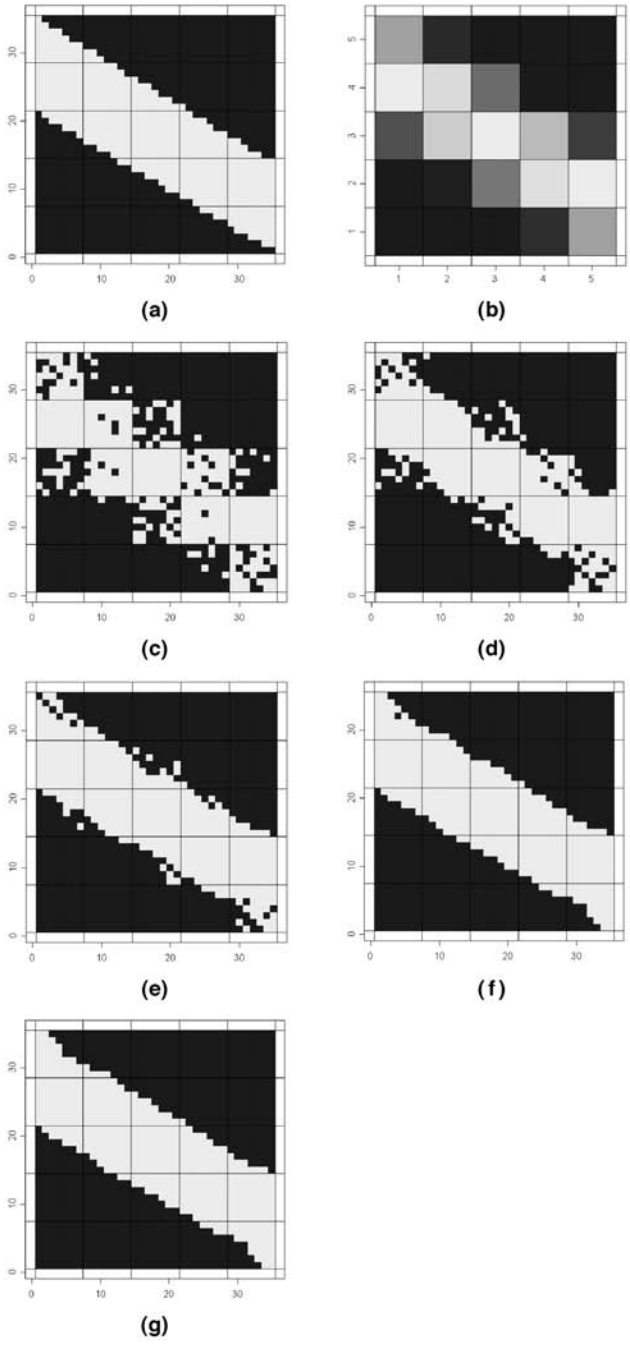

Figure 2. Sub-pixel mapping of a linear feature: (a) test image, (b) image of proportions input to the algorithm, (c) random initial allocation to sub-pixels, (d) solution after three iterations, (e) solution after six iterations, (f) solution after nine iterations, and (g) solution after 12 iterations. (Used with permission by Springer Europe NL)

and grassland classes were amalgamated into one class (non-woodland). The resulting image is shown in Figure 4a.

The classified image was filtered (7 pixel by 7 pixel majority filter) to reduce local mis-classification error. The image was then spatially degraded by a zoom factor of 8 to a spatial resolution of 32 m by 32 m (approximately equal to that of Landsat Thematic Mapper imagery, that is, 30 m by 30 m). At the coarser spatial resolution of 32 m by 32 m, the contribution of each sub-pixel was summed to obtain a pixel-level proportion for each class (Figure 4b). These pixel proportions then formed the input to the sub-pixel mapping algorithm. Two advantages of the above approach are (a) the ability to evaluate the sub-pixel mapping exhaustively because the target image is known, and (b) the ability to focus on the mapping algorithm rather than the soft classifier that would in practice predict the class proportions.

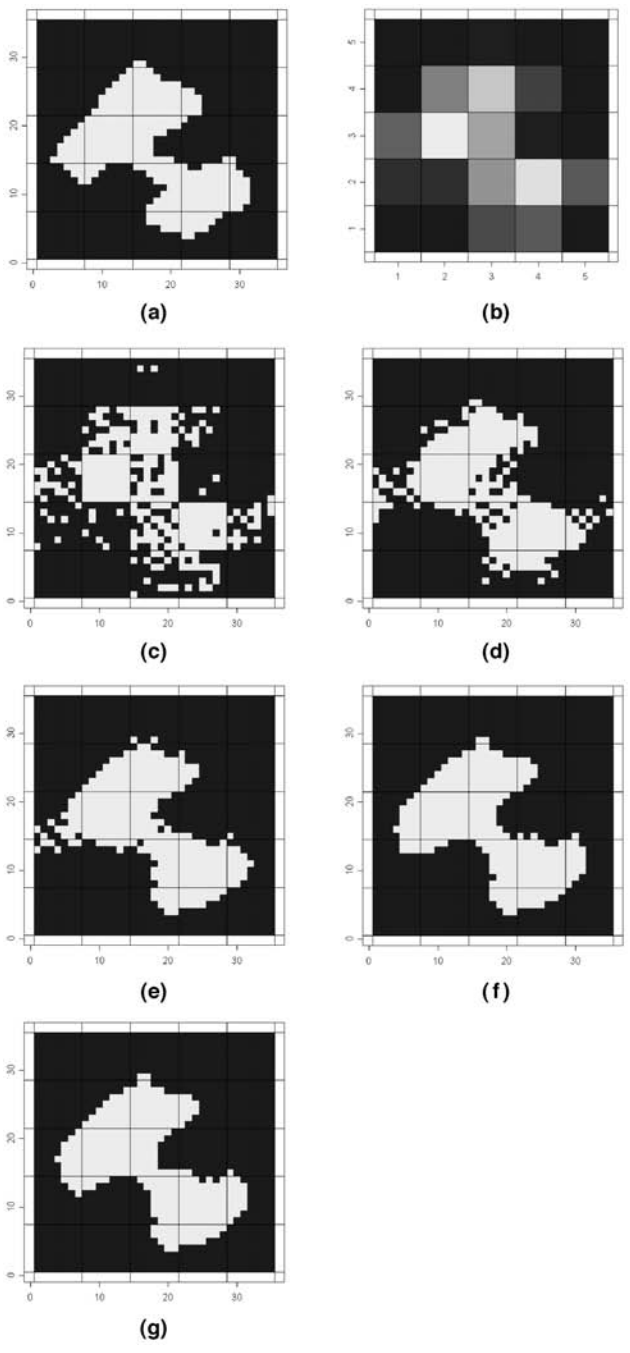

Figure 3. Sub-pixel mapping of an irregular polygon: (a) test image, (b) image of proportions input to the algorithm, (c) random initial allocation to sub-pixels, (d) solution after five iterations, (e) solution after 10 iterations, (f) solution after 15 iterations, and (g) solution after 20 iterations.

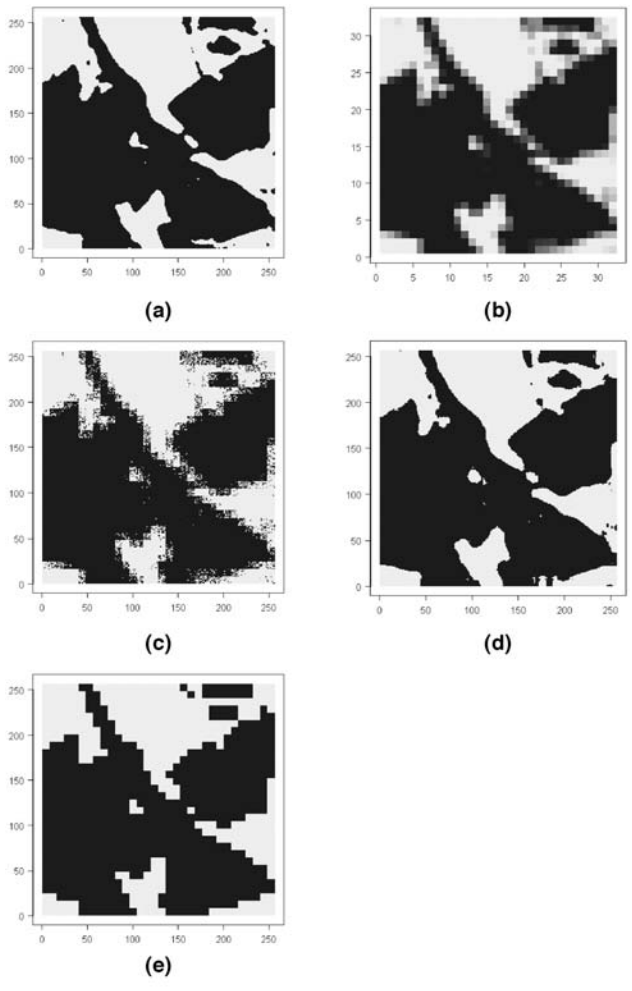

Figure 4. Sub-pixel mapping applied to a classified Ikonos image of Chandler's Ford, Hampshire spatially degraded to a spatial resolution of 32 m: (a) test image (spatial resolution of 4 m), (b) image of proportions input to the algorithm (spatial resolution of 32 m), (c) random initial allocation to sub-pixels (spatial resolution of 4 m), (d) solution after 50 iterations (spatial resolution of 4 m), and (e) hard classification for comparison (spatial resolution of 32 m).

Analysis

Simple Targets

Given the two input images of pixel-level proportions, the algorithm initially allocated each sub-pixel to a binary hard class randomly, such as to maintain the original pixel proportions (Figure 1c and Figure 2c). Thereafter, the algorithm made a maximum of one swap per-pixel for each iteration. The number of nearest neighbors used was 2 (i.e., the clique was second-order), and the non-linear parameter of the exponential model a was set to 5 pixels. For each of the simple images shown in Figure 1 and Figure 2 less than ten iterations was sufficient to achieve convergence.

For the circle, the overall accuracy of the predicted image increased with each iteration of the algorithm until convergence. The overall accuracy of the final predicted image (Figure 1g) was 100 percent (i.e., perfect reconstruction), compared to an overall accuracy of 88 percent for the initial random allocation (Figure 1c). This result is comparable to that of Tatem *et al.* (2001a). The circle is the most compact two-dimensional shape and, thus, it is the easiest for the algorithm to reproduce.

For the linear feature (Figure 2) the result was also acceptable visually. Again, the overall accuracy increased with each iteration until convergence. The overall accuracy of the final predicted image (Figures 2g) is 99 percent, compared to an overall accuracy of 86 percent for the initial random

allocation (Figure 2c). It is worth noting that the edge effect apparent in Tatem *et al.* (2001a) did not occur here because the algorithm was coded to ignore the boundary. Thus, it appears that the simple algorithm is capable of producing excellent results, at least for simple geometric shapes.

Polygonal Target

The algorithm was applied to the image of proportions shown in Figure 3b. Initially, the proportions per-pixel were used to allocate hard binary classes to the sub-pixels within each pixel (Figure 3c). Then, the algorithm proceeded iteratively to converge on a solution. Convergence was reached in around 15 iterations. This time the differences between the predicted image and the target image were more obvious. This is reflected in the overall accuracy which does not increase to as large a value as for the simple shapes. Nevertheless, a large increase in accuracy relative to the initial random allocation was achieved (96 percent compared to 84 percent). Thus, even for this more complex shape, the algorithm does result in an increase in per-sub-pixel accuracy.

Application to Ikonos Imagery

The pixel-swapping algorithm was applied to the 32 pixel by 32 pixel degraded Ikonos image of class proportions (Figure 4b). Initially, the sub-pixels within each pixel were allocated to one of the two classes as previously described (Figure 4c). The non-linear parameter of the exponential model was set to five pixels and the bandwidth was set to five pixels. The algorithm was run for 50 iterations. The resulting sub-pixel map is shown in Figure 4d. The per-sub-pixel accuracy of the sub-pixel map was 98.4 percent, which is very high in a remote sensing context (Foody, 2002). In comparison, the overall accuracy of the initial random allocation was 93.2 percent, 5.2 percent less than the sub-pixel map. This difference, while small, is large when viewed relative to the amount of mis-classification (i.e., a 5.2 percent increase in accuracy relative to a 6.8 percent classification error amounts to a 76 percent reduction in mis-classification).

For comparison with the sub-pixel map, a hard classification was simulated from the proportions image by allocating each pixel to the class with the largest cover proportion (Figure 4e). This image can be thought of as analogous to the output from a hard (e.g., maximum likelihood) classifier applied at the pixel-level. The per-sub-pixel accuracy of the hard classified image (Figure 4e) was 94.9 percent. The increase in accuracy achieved by sub-pixel mapping is readily apparent from a visual comparison of Figure 5d and Figure 5e. The hard classified image has an unnatural blocky appearance, and some features are mis-represented. Moreover, certain small features that exist in the target image (Figure 4a) are represented well in the sub-pixel map, but are absent from the hard classified image.

Discussion

Limitations

The proposed algorithm produced excellent results for a set of simple simulated shapes and a real classified Ikonos image. However, there are certain conditions under which the algorithm would not be expected to perform accurately. First, it is assumed that the classes found in the scene can be well represented as a crisp set. That is, the boundaries in the scene to be predicted from imagery are sharply defined. If a fuzzy set more appropriately represents the classes in the scene, such that mixed pixels arise through vagueness (rather than ambiguity), then the algorithm proposed in this paper would be inappropriate. Second, the algorithm attempts to maximize the spatial correlation between neighboring sub-pixels. No information on the direction of variation is used, so that the algorithm tends to produce compact convex shapes. The algorithm, at least as presented here, is not appropriate for features that do not fit this description (e.g., linear features such as roads and waterways). Third, the algorithm requires some spatial correlation between pixels. This implies that the proposed algorithm is suitable only for mapping objects that are larger than a pixel. Where multiple small objects are present within a pixel, the algorithm will incorrectly predict a single larger object by coalescing the smaller objects. To map objects that are smaller than a pixel, an alternative algorithm must be defined.

Comparison to spatial simulated annealing

The algorithm presented in this paper is simple and efficient. However, there are several important differences between its implementation here and the implementation of spatial simulated annealing (SSA) algorithms (Deutsch and Journel, 1998; van Groenigen, 1999).

First, the SSA-type algorithm is based on the random selection of two sites and their swapping, if the value of some objective function is increased as a result of the swap. In the present algorithm the entire image of some distance weighted function is calculated, and the two most eligible (in terms of $A(\cdot)$) sites are swapped, conditional upon the swap resulting in an increase in spatial correlation between sub-pixels. This difference makes the present algorithm process very fast.

Another important difference between the present algorithm and SSA is that the present algorithm has no stochastic element (the random initialization aside). A consequence of this may be that for larger, more complex shapes, there is a greater likelihood of falling into local minima. However, it is believed that the likelihood of this occurring is low because (a) only one sub-pixel swap is made per pixel per iteration, and (b) the swaps are limited to pixels (cannot be made between pixels) such that the solution is already somewhat constrained. For the features shown in Figures 1 through 3, several runs (with different initial sub-pixel allocations) resulted in the same predicted images, but this may not be the case for more complex shapes. In the future, SSA-type algorithms will be implemented and compared to the present algorithm.

Choice of Parameters

Several parameters (including the choice of distance-weighted function) needed to be set by the investigator, and of these, the most important was the number of neighbors and the non-linear parameter of the exponential function. The number of neighbors was initially set to one to increase the speed of the algorithm, but this was found to produce unsatisfactory results. The number of neighbors was set to two for the simulated images (Figures 1 through 3) and five for the Ikonos image (Figure 4). An important consideration is that the number of neighbors should not be so large that a given sub-pixel is attracted to other sub-pixels that it cannot neighbor (e.g., belonging to a feature that exists in a pixel that its own pixel does not neighbor). Thus, the maximum non-linear parameter should always be, at most, one sub-pixel less than the number of sub-pixels along a pixel side.

The zoom factor represents another important parameter that must be set by the investigator. The zoom factor is the relative increase in spatial resolution from the pixel-level image of proportions to the sub-pixel level image of hard land cover classes. In the examples presented in this paper, the zoom factor was equal to seven (or eight for the Ikonos image). This number was chosen because it has been used previously by Tatem *et al.* (2001a), and because it allowed

rapid development of the algorithm. However, any zoom factor, including larger factors, could have been chosen. The results of Tatem *et al.* (2001a) suggest that larger zoom factors increase the precision of prediction.

Potential Applications in Remote Sensing

The algorithm implemented here has great potential for detecting targets in remotely sensed imagery. For example, potential applications include prediction of flood envelopes (i.e., delineation of flood boundaries) from remotely sensed imagery, mapping of ice flows in relatively coarse spatial resolution imagery, and mapping of vehicles and buildings using high spatial resolution imagery.

Conclusions

Sub-pixel mapping, as embodied in the algorithm introduced in this paper, represents an important step from soft classification. The output from a soft classification is a map of land cover proportions defined at the pixel-scale. Sub-pixel mapping takes that output and transforms it into a map of hard land cover classes defined at the sub-pixel scale. The results are more informative, easier to interpret, and more accurate (on a per-sub-pixel by per-sub-pixel basis) at no extra data cost.

A simple, efficient algorithm has been presented as an alternative to the HNN algorithm for sub-pixel target mapping in remotely sensed imagery. The HNN algorithm is not particularly accessible to the remote sensing practitioner, whereas the algorithm demonstrated here can be coded readily in any scientific computing language. In its present form, it allows the mapping of hard binary land cover (target, non-target) classes at a finer spatial resolution from soft land cover proportions at an original spatial resolution. The algorithm was demonstrated to produce excellent results for three simple images and one complex image.

Additional research is necessary to define an algorithm for mapping objects that are smaller than a pixel, to extend the current algorithm to handle multiple land cover classes simultaneously, and to define alternative algorithms (e.g., SSA-type algorithms) for sub-pixel mapping.

References

Adams, J.B., M.O. Smith, and P.E. Johnson, 1985. Spectral mixture modelling: a new analysis of rock and soil types at the Viking Lander 1 site, *Journal of Geophysical Research*, 91:8098–8112.

Aplin, P., and P.M. Atkinson, 2001. Sub-pixel land cover mapping for per-field classification, *International Journal of Remote Sensing*, 22:2853–2858.

Atkinson, P.M., 1997. Mapping sub-pixel boundaries from remotely sensed images, *Innovations in GIS IV* (Z. Kemp, editor), Taylor and Francis, London, pp. 166–180.

Atkinson, P.M., and P.J. Curran, 1997. Choosing an appropriate spatial resolution for remote sensing investigations, *Photogrammetric Engineering & Remote Sensing*, 63:1345–1351.

Atkinson, P.M., M.E.J. Cutler, and H. Lewis, 1997. Mapping sub-pixel proportional land cover with AVHRR imagery, *International Journal of Remote Sensing*, 18:917–935.

Atkinson, P.M., and N.J. Tate, 2000. Spatial scale problems and geostatistical solutions: a review, *Professional Geographer*, 52:607–623.

Atkinson, P.M., and A.R. Tatnall, 1997. Introduction: neural networks in remote sensing, *International Journal of Remote Sensing*, 18:699–709.

Benediktsson, J.A., P.H. Swain, and O.K. Ersoy, 1990. Neural network approaches versus statistical methods in classification of multisource remote sensing data, *IEEE Transactions on Geoscience and Remote Sensing*, 28:540–552.

Bezdek, J.C., 1981. *Pattern Recognition with Fuzzy Objective Function Algorithms*, Plenum Press, New York.

Bezdek, J.C., R. Ehrlich, and W. Full, 1984. FCM: The fuzzy *c*-means clustering algorithm, *Computers and Geosciences*, 10:191–203.

Brown, M., S.R. Gunn, and H.G. Lewis, 1999. Support vector machines for optimal classification and spectral unmixing, *Ecological Modelling*, 120:167–179.

Chiles, J.-P., and P. Delfiner, 1999. *Geostatistics. Modeling Spatial Uncertainty*, Wiley, New York, 695 p.

Congalton, R.G., 1991. A review of assessing the accuracy of classifications of remotely sensed data, *Remote Sensing of Environment*, 37:35–46.

Curran, P.J., and P.M. Atkinson, 1998. Geostatistics and remote sensing, *Progress in Physical Geography*, 22:61–78.

Deutsch, C.V., and A.G. Journel, 1998. *GSLIB: Geostatistical Software and User's Guide*, Second Edition, Oxford University Press, Oxford.

Flack, J., M. Gahegan, and G. West, 1994. The use of sub-pixel measures to improve the classification of remotely sensed imagery of agricultural land, *Proceedings of the 7th* Australasian Remote Sensing Conference, Melbourne, pp. 531–541.

Foody, G.M., 1998. Sharpening fuzzy classification output to refine the representation of sub-pixel land cover distribution, *International Journal of Remote Sensing*, 19:2593–2599.

Foody, G.M., 2002. Status of land cover classification accuracy assessment, *Remote Sensing of Environment*, 80:185–201.

Foody, G.M., and D.P. Cox, 1994. Sub-pixel land cover composition estimation using a linear mixture model and fuzzy membership functions, *International Journal of Remote Sensing*, 15:619–631.

Garcia-Haro, F.J., M.A. Gilabert, and J. Melia, 1996. Linear spectral mixture modelling to estimate vegetation amount from optical spectral data, *International Journal of Remote Sensing*, 17:3373–3400.

Gillespie, A.R., 1992. Spectral mixture analysis of multi-spectral thermal infrared images, *Remote Sensing of Environment*, 42:137–145.

Goovaerts, P., 1997. *Geostatistics for Natural Resources Evaluation*, Oxford University Press, New York.

Hopfield, J.J., and D.W. Tank, 1985. "Neural" computation of decisions in optimization problems, *Biological Cybernetics*, 52:141–152.

Jupp, D.L.B., A.H. Strahler, and C.E. Woodcock, 1988. Autocorrelation and regularization in digital images I: Basic theory, *IEEE Transactions on Geoscience and Remote Sensing*, 26:463–473.

Jupp, D.L.B., A.H. Strahler, and C.E. Woodcock, 1989. Autocorrelation and regularization in digital images II: Simple image models, *IEEE Transactions on Geoscience and Remote Sensing*, 27:247–258.

Justice, C.O., and J.R.G. Townshend, 1981. Integrating ground data with remote sensing, *Terrain Analysis and Remote Sensing* (J.R.G. Townshend, editor), Allen and Unwin, London, pp. 38–101.

Mason, D.C., D.M. Cobby, M.S. Horritt, and P.D. Bates, 2003. Floodplain friction parameterization in two-dimensional river flood models using vegetation heights derived from airborne scanning laser altimetry, *Hydrological Processes*, 17:1711–1732.

Matheron, G., 1965. *Les Variables Régionalisées et Leur Estimation*, Masson, Paris.

Paola, J.D., and R.D. Schowengerdt, 1995. Review article: A review and analysis of backpropagation neural networks for classification of remotely sensed multispectral imagery, *International Journal of Remote Sensing*, 16:3033–3058.

Schneider, W., 1993. Land use mapping with subpixel accuracy from landsat TM image data, *Proceedings of the 25th* International Symposium on Remote Sensing and Global Environmental Change, pp. 155–161.

Schneider, W., 1999. Land cover mapping from optical satellite images employing subpixel segmentation and radiometric calibration, *Machine Vision and Advanced Image Processing in Remote Sensing* (I. Kanellopoulos, G. Wilkinson, and T. Moons, editors), Springer, London.

Steinwendner, J., W. Schneider, and F. Suppan, 1998. Vector segmentation using spatial subpixel analysis for object extraction, *International Archives of Photogrammetry and Remote Sensing*, 32:265–271.

Tate, N.J., and P.M. Atkinson, 2001. *Modelling Scale in Geographical Information Science*, Wiley, Chichester, pp. 277.

Tatem, A.J., H.G. Lewis, P.M. Atkinson, and M.S. Nixon, 2001a. Sub-pixel target identification from remotely sensed images using a Hopfield neural network, *IEEE Transactions on Geoscience and Remote Sensing*, 39:781–796.

Tatem, A.J., H.G. Lewis, P.M. Atkinson, and M.S. Nixon, 2001b. Multiple class land cover mapping at the sub-pixel scale using a Hopfield neural network, *International Journal of Applied Earth Observation and Geoinformation*, 3:184–190.

Thomas, I., V. Benning, and N.P. Ching, 1987. *Classification of Remotely Sensed Images*, Adam Hilger, Bristol.

van den Hurk, B.J.J.M., P. Viterbo, and S.O. Los, 2003. Impact of leaf area index seasonality on the annual land surface evaporation in a global circulation model, *Journal of Geophysical Research-Atmospheres*, 108 (D6), Article Number 4191.

Verhoeye J., and R. De Wulf, 2002. Land cover mapping at sub-pixel scales using linear optimization techniques, *Remote Sensing of Environment*, 79:96–104.

Van Groenigen, J.-W., 1999. *Constrained Optimisation of Spatial Sampling. A Geostatistical Approach*, ITC Publication Series, No. 65, ITC, Enschede, the Netherlands.

Wilson, M.D., and P.M. Atkinson, 2003. Sensitivity of a flood inundation model to spatially-distributed friction, *IEEE International Geoscience and Remote Sensing Symposium 2003*, unpaginated CD-ROM.

Woodcock, C.E., and A.H. Strahler, 1987. The factor of scale in remote sensing, *Remote Sensing of Environment*, 21:311–322.

Zhan, Q., M. Molenaar, and A. Lucieer, 2002. Pixel unmixing at the sub-pixel scale based on land cover class probabilities: application to urban areas, *Uncertainty in Remote Sensing and GIS* (G.M. Foody and P.M. Atkinson, editors), Wiley: Chichester, pp. 59–76.

(Received 26 February 2004; accepted 06 April 2004; revised 04 May 2004)